Hindawi
Geofluids
Volume 2019, Article ID 1853274, 21 pages
https://doi.org/10.1155/2019/1853274

Research Article

Numerical Simulation of the Influence of Geological CO_2 Storage on the Hydrodynamic Field of a Reservoir

Zhaoxu Mi,[1] Fugang Wang,[1] Zhijie Yang,[1] Xufeng Li,[2] Yujie Diao,[2] Xin Ma,[2] and Hailong Tian[1]

[1]*Key Laboratory of Groundwater Resources and Environment, Ministry of Education, Jilin University, Changchun 130012, China*
[2]*Key Laboratory of Carbon Dioxide Geological Storage, Center for Hydrogeology and Environmental Geology Survey, China Geological Survey, Baoding, Hebei 071051, China*

Correspondence should be addressed to Fugang Wang; wangfugang@jlu.edu.cn

Received 20 July 2018; Revised 18 March 2019; Accepted 7 May 2019; Published 2 June 2019

Guest Editor: Bisheng Wu

CO_2 geological storage in deep saline aquifers is an effective way to reduce CO_2 emissions. The injection of CO_2 inevitably causes a significant pressure increase in reservoirs. When there exist faults which cut through a deep reservoir and shallow aquifer system, there is a risk of the shallow aquifer being impacted by the changes in reservoir hydrodynamic fields. In this paper, a radial model and a 3D model are established by TOUGH2-ECO2N for the reservoir system in the CO_2 geological storage demonstration site in the Junggar Basin to analyze the impact of the CO_2 injection on the deep reservoir pressure field and the possible influence on the surrounding shallow groundwater sources. According to the results, the influence of CO_2 injection on the reservoir pressure field in different periods and different numbers of well is analyzed. The result shows that the number of injection wells has a significant impact on the reservoir pressure field changes. The greater the number of injection wells is, the greater the pressure field changes. However, after the cessation of CO_2 injection, the number of injection wells has little impact on the reservoir pressure recovery time. Under the geological conditions of the site and the constant injection pressure, although the CO_2 injection has a significant influence on the pressure field in the deep reservoir, the impact on the shallow groundwater source area is minimal and can be neglected and the existing shallow groundwater sources are safe in the given project scenarios.

1. Introduction

Global warming presents a serious threat to the living environment of humans. Reducing the emissions of carbon dioxide (CO_2) is a common challenge for countries worldwide [1]. The geological storage of CO_2 has attracted the attention of governments and scientists around the world as a direct and effective emission reduction method recognized by the international community [2–5]. Once the CO_2 has been transported, it is stored in porous geological formations that are typically located several kilometers below the Earth's surface, and under the pressure and temperature conditions of such reservoirs, CO_2 exists in a dense phase. Suitable storage sites include former gas and oil fields, deep saline formations, or nearly depleted oil fields where the injected carbon dioxide may increase the amount of oil recovered. The storage mechanism includes structural storage, residual storage, dissolution storage, and mineral storage. The geological storage of CO_2 is a complex process and is therefore affected by many factors, such as the reservoir conditions, rock heterogeneity, faults, minerals, relative permeability hysteresis, and dip angle of the reservoir[6–9]. Because deep saline aquifers can be found in widespread areas, these aquifers are considered to have enormous potential for CO_2 storage [1]. Therefore, deep saline aquifers have received much attention as places to store CO_2.

For the large-scale injection of CO_2, the increase in pressure is a major factor affecting the storage capacity and storage safety [10–12]. Two important potential risks associated with the pressure increase have attracted the attention of many scholars. The first risk involves geomechanical effects, such as caprock fracturing, fault resurrection, and induced earthquakes. The second risk involves environmental impacts, such as the impacts on shallow aquifers and

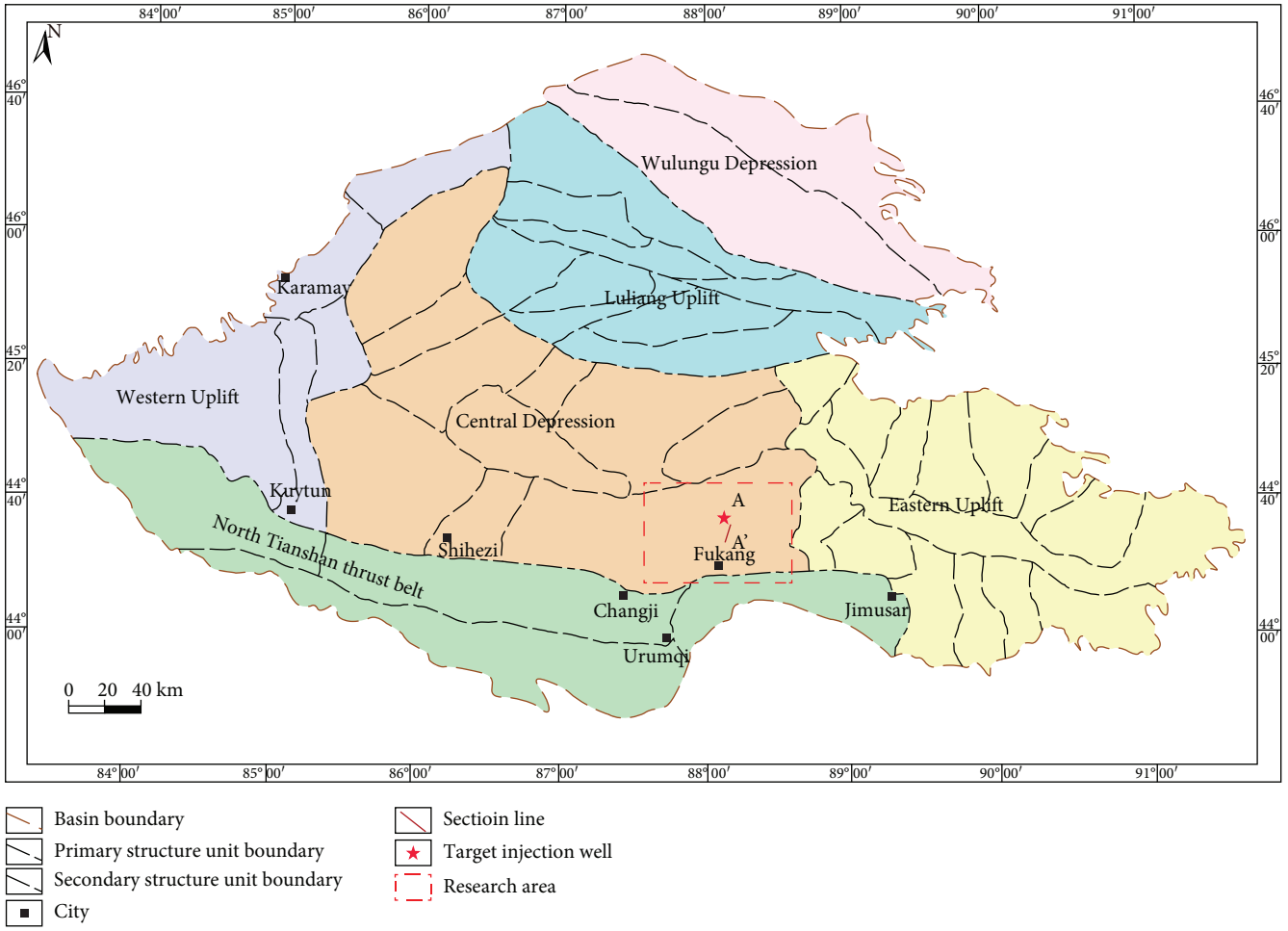

Figure 1: Division of the tectonic units in the Junggar Basin [22, 23].

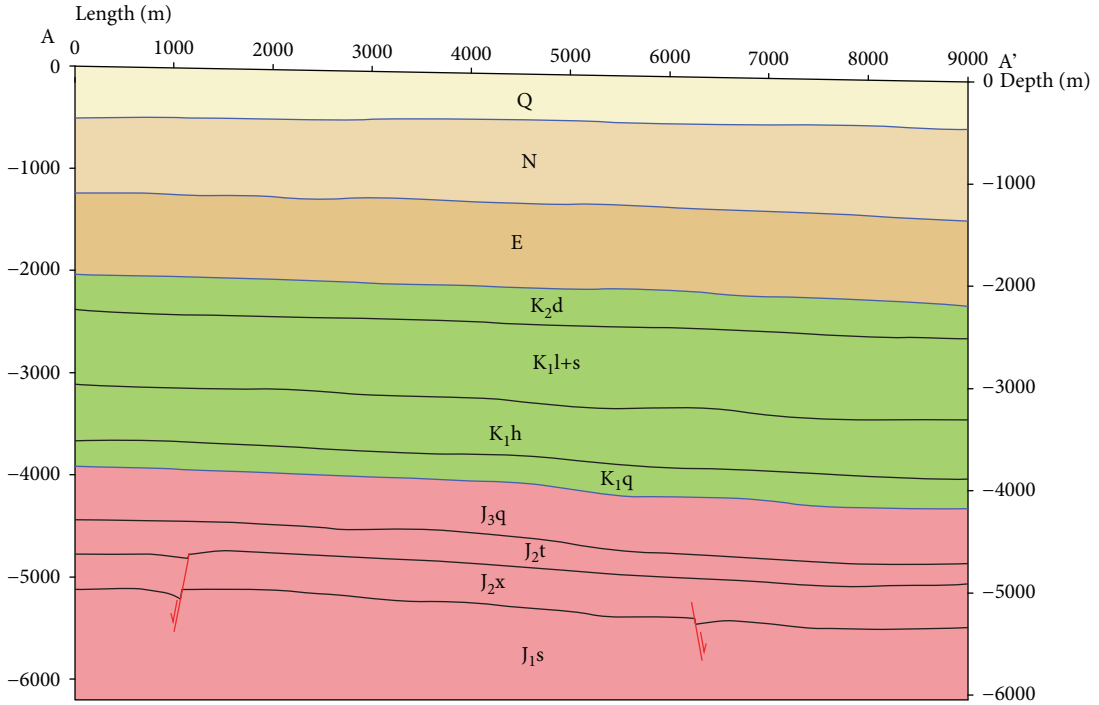

Figure 2: Geological profile near the target injection well (see the location of the profile in Figure 1).

Era	System	Series	Formation	Thickness (m)	Column	Lithological description
Cenozoic	Quaternary	—	(Q)	350		Gray, light-yellow, earthy-yellow quartz sand, with minor clay
	Neogene	—	(N)	1055		Grayish-yellow mudstone and siltstone
	Paleocene	—	(E)	525		Brown-red, taupe argillite and siltstone
Mesozoic	Cretaceous	Upper	Donggou (K_2d)	356		Brown-red, mauve mudstone with siltstone
		Lower	Lianmuqin + Shengjinkou (K_1l+s)	729		Brown-red, mauve mudstone, and gray muddy siltstone
			Hutubi (K_1h)	573		Brown mudstone, sandy mudstone, and gray siltstone
			Qingshuihe (K_1q)	288		Brown mudstone and gray fine sandstone
	Jurassic	Upper	Qigu (J_3q)	418		Maroon mudstone and siltstone
		Middle	Toutunhe (J_2t)	296		Gray mudstone and gray siltstone
			Xishanyao (J_2x)	377		Dark-gray mudstone with grey siltstone and black coal seam
		Lower	Sangonghe (J_1s)	438		Dark-gray sandy mudstone, and gray pebbly sandstone

Figure 3: Lithological column of the target injection well.

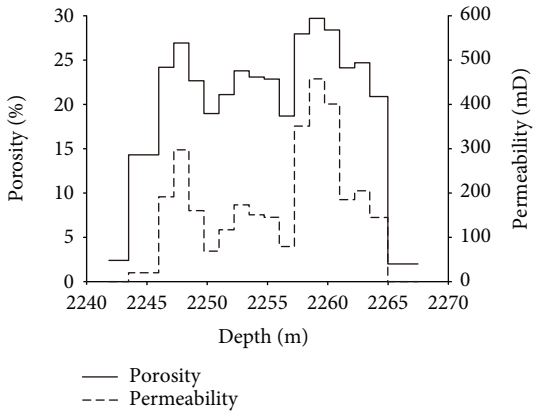

Figure 4: Porosity and permeability of the reservoir strata.

existing underground development activities resulting from the pressure-induced leakage of CO_2 and salt water [13–15].

Nicot [16] studied large CO_2 injections into aquifers along the coast of the Gulf of Mexico. They found that an amount equivalent to 50 million tons of CO_2 per year for 50 years resulted in an average water table rise of 1 m. In a study on CO_2 injection in the Illinois Basin, Birkholzer and Zhou [17] demonstrated that multiple-site storage in the Mount Simon Sandstone would result in a large continuous overpressurized region. With respect to far-field impacts, pressure changes may propagate as far as 200 km from the core injection area hosting the 20 storage sites. Zhao et al. [18] simulated the use of 20 wells in the Songliao Basin to continuously inject CO_2 at different rates. After 50 years, the formation pressure increased by 8.62 MPa. Yamamoto et al. [19] simulated the impact of industrial-scale perfusion of CO_2 in Tokyo Bay, Japan, on pressure increase and

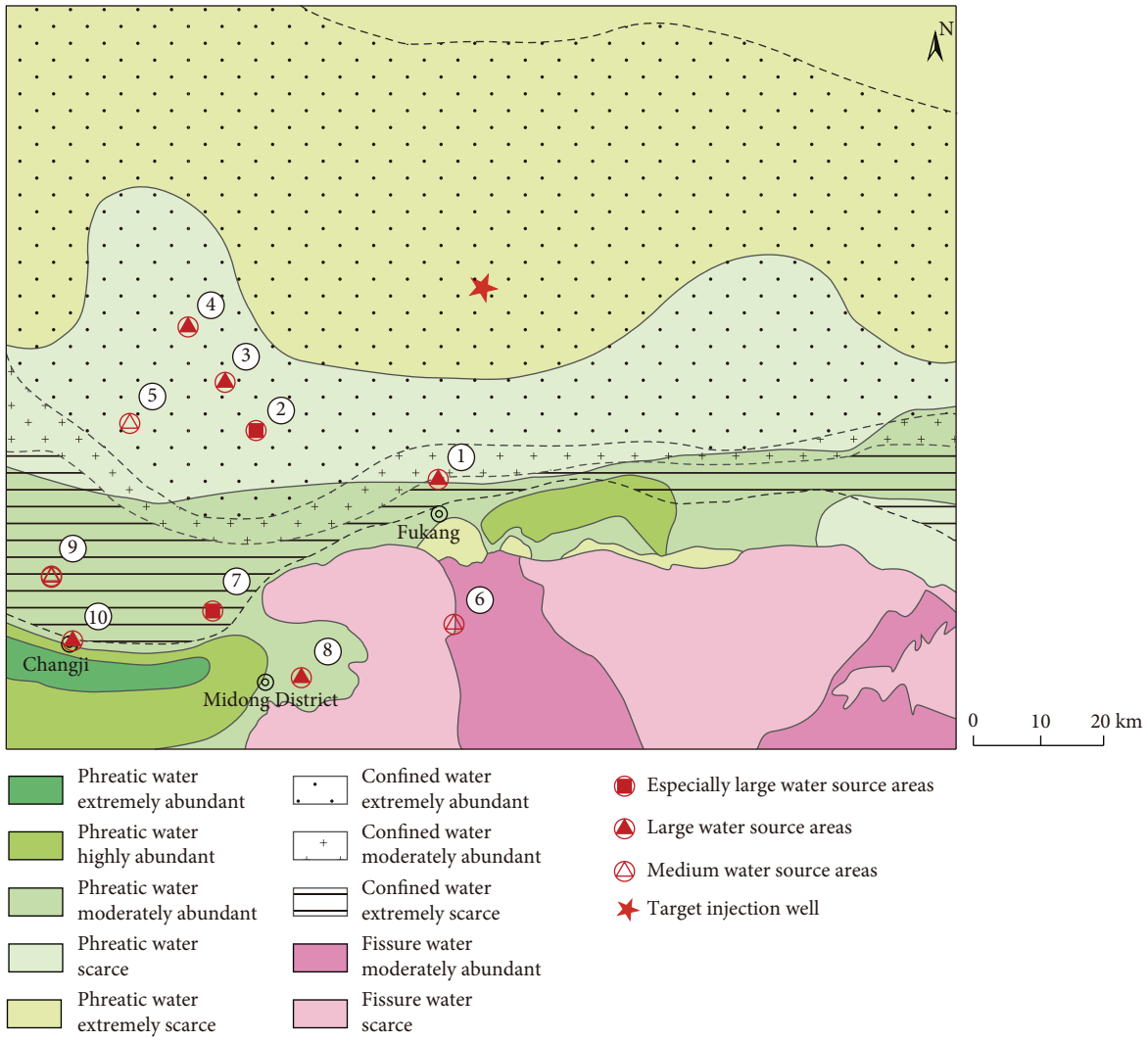

Figure 5: Hydrogeological conditions and distribution of groundwater sources in the study area.

groundwater relocation using 10 injection wells and the injection of 100 million tons per year for 100 years, which caused CO_2 plumes to spread for several kilometers. Birkholzer et al. [17, 20] argued that numerical simulations of large industrial-scale carbon capture and storage (CCS) projects show that pressure changes caused by CO_2 injection may spread far within a CO_2 reservoir and may even affect the entire reservoir and basin.

The availability of water resources seriously affects the economic development and ecological environment in the southern part of the Junggar Basin. The implementation of the CCS demonstration project located to the north of Fukang will affect the water quality and hydrodynamic field of the groundwater. In this paper, the influence of CO_2 injection on the reservoir pressure field is systematically explored through numerical simulation by TOUGH2-ECO2N to analyze the impact of the CO_2 injection on the deep reservoir pressure field and the possible influence on the surrounding shallow groundwater sources. The impact of large-scale CO_2 injection on groundwater development and the shallow surrounding water sources was analyzed under conditions of different numbers of injection wells. This study provides a basis for the CO_2 geological storage project and safety of groundwater sources in the Junggar Basin.

2. Geological Characteristics of the Study Area

The Junggar Basin is located in the northern Xinjiang Uygur Autonomous Region in China. This basin is the second largest inland basin in China, with a total area of approximately 135000 km^2. According to the late Paleozoic tectonic characteristics, the Junggar Basin is divided into six first-order tectonic units, namely, the Wulungu Depression, Luliang Uplift, Western Uplift, Central Depression, Eastern Uplift, and North Tian Shan thrust belt, and 44 secondary tectonic units. The division of tectonic units in the Junggar Basin is shown in Figure 1. The Junggar Basin is an important energy base in China and is rich in coal, oil, natural gas, and other resources. The northern slope of the Tian Shan Mountains in the southern part of the basin is one of the most developed regions in Xinjiang, China. The basin is one of the key areas for the development of western China.

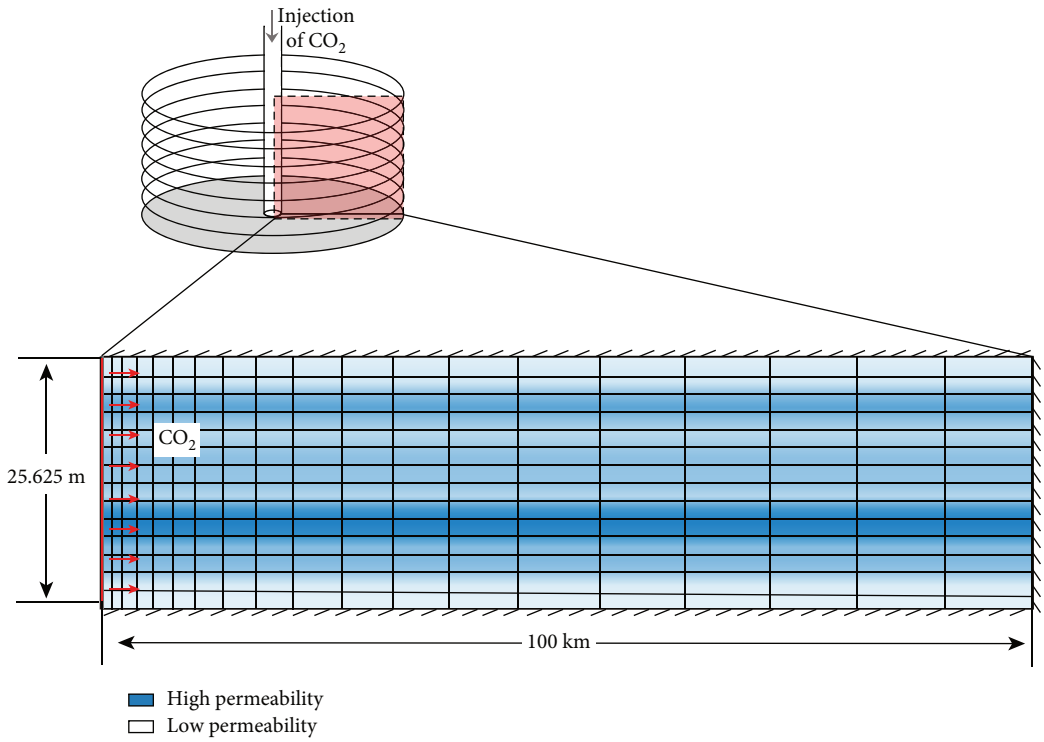

Figure 6: Schematic diagram of the radial model for CO_2 injection.

83% of the heavy industry and 62% of the light industry of Xinjiang are concentrated in this region. A large number of coal-fired power plants, steel mills, and coal-based chemical industries are located in Xinjiang and are the major sources of CO_2 emissions [21].

The study area is the CO_2-enhanced saline water recovery demonstration site in the eastern part of the Junggar Basin, located on the northern side of the Tian Shan Mountains and approximately 30 km from Fukang, as shown in Figure 1. The geological structure is located in the northeastern Fukang Depression. The sedimentary strata, similar to those throughout the entire basin, experienced various tectonic events from the late Paleozoic to the Quaternary related to the Hercynian, Indosinian, Yanshanian, and Himalayan orogenies. The geological section of the study area near the injection well is shown in Figure 2, and a stratigraphic column of the target injection well is shown in Figure 3. The target layer in this study is the Cretaceous Donggou Formation (K_2d).

According to the porosity and permeability test data from the target injection well, the relatively high-porosity and high-permeability Donggou Formation was selected as the target reservoir in this study. Above and below the target reservoir, there are formations with low porosity and permeability values to act as the caprocks. The burial depth range of the target strata is determined based on the data from the target well at the demonstration site, which is shown in Figure 4.

The groundwater sources in the study area are located at the southern edge of the Junggar Basin and the northern foot of the Tian Shan Mountains. With economic development, the demand for water resources is increasing. The development and utilization of groundwater have greatly increased. In the south and west of the study area, there are several large water sources. Water source #1 in the south of the study area is the closest one to the injection well, with a distance of approximately 25 km. The distances between the injection well and sources #2, #3, and #4 to the southwest are all approximately 35 km. The groundwater sources extract water from the Quaternary pore aquifer system and shallow bedrock-confined aquifers [24] (Figure 5). With the increase in the amount of groundwater development, the groundwater environment is constantly deteriorating. This situation has led to a series of ecological and environmental problems, such as groundwater overexploitation, vegetation degradation, water quality deterioration, and desertification. The exploitation and protection of groundwater are of great significance to the lives and economic development of the local people. With the implementation of the CO_2 geological storage project located to the northeast of the groundwater source area, CO_2 will migrate to the surrounding area from the injection wells. Although the existing groundwater sources are about 30 km away from the injection well and the vertical distance between the water source-extracted aquifer and the deep reservoir is about 1600 m, there still is the possibility that the groundwater sources are impacted by the injection project for their location near the Tian Shan piedmont fault zone. According to the early geological survey, the scale of the faults is large. The possible impact of the deep reservoir on the shallow aquifer system is from the large faults which might cut through different strata. When the pressure field of the deep reservoir has a significant change, it might affect the shallow groundwater source

(a) (b)

(c)

Figure 7: Rock samples from the Donggou Formation for parameter testing.

Table 1: Parameters of rock used in the model.

Parameter	Value
Rock density	2600 kg/m^3
Thermal conductivity	2.51 W/m·°C
Rock grain specific heat	920 J/kg·°C
Aquifer initial pressure	22.50 MPa
Aquifer initial temperature	63.0°C
Total dissolved solids (TDS)	43223.05 mg/L

Table 2: Definitions for parameters.

Parameter	Definition	Value
k_{rl}	Liquid relative permeability	Equation (1)
S_l	Liquid saturation	—
S_{lr}	Residual liquid saturation	0.30
m	Empirical coefficient	0.457
S_{ls}	Maximum liquid saturation	0.90
k_{rg}	Gas relative permeability	Equation (3)
S_{gr}	Residual gas saturation	0.05
P_{cap}	Capillary pressure	Equation (5)
P_0	Breakthrough pressure	19.61 kPa
λ	Empirical coefficient	0.457

safety by the possible connection via the faults. There is a risk of CO_2 entering the groundwater sources and contaminating the groundwater. Once CO_2 enters the water sources, serious consequences may occur, such as the acidification of the groundwater and the release of heavy metal elements into the aquifer. Additionally, the impact of large-

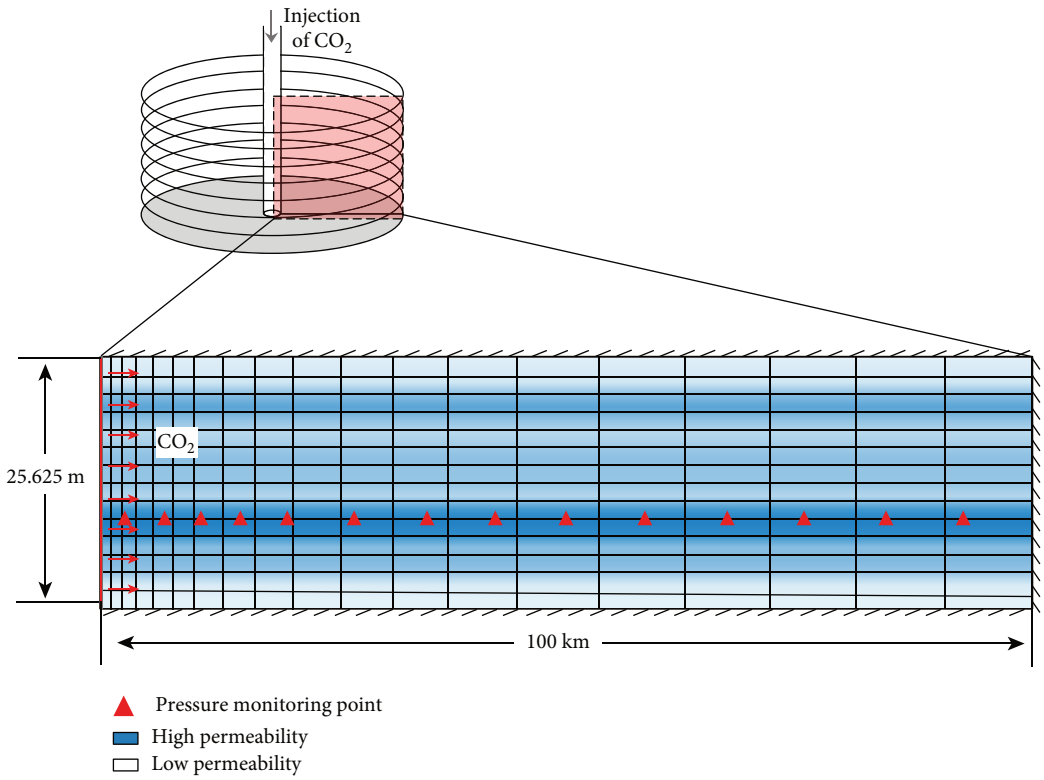

Figure 8: Positions of the pressure monitoring points in the radial model.

scale CO_2 injection on the reservoir pressure field may also lead to changes in the hydrodynamic field of the aquifer associated to the water sources, which could cause groundwater safety problems.

The target reservoir in the Donggou Formation is distributed across the entire study area. The formation is gently undulating and has an inclination of approximately 0° to 3°. The formation is shallower in the northeast and deeper in the southwest. This formation unconformably overlies the Cretaceous Lianmuqin and Shengjinkou Formations. This formation was deposited in a river delta sedimentary environment. The lithology is interbedded sandstone and mudstone. This study selected one of the perforation sections of the Donggou Formation reservoir with a burial depth of 2241.855-2267.48 m. The thickness of this section is 25.625 m. According to the actual measured value in the target injection well, the temperature at the bottom of the reservoir is 63.0°C and the initial pressure is 22.50 MPa.

3. Numerical Simulation Study

In CO_2 geological storage projects, the injection of CO_2 into deep saline aquifers causes the pressure in the reservoir to rise [16, 18, 20, 25]. In the numerical simulation study of geological fluid diffusion in complex geological structures, a complex 3D geological model is generally established to more scientifically represent practical problems. However, as the scale of the 3D simulation model increases, the computing time increases significantly. Therefore, in the actual simulation, the scientific and reasonable selection of the model scale is an important issue. In the case of CO_2 injection, the basin boundary is characterized as infinite relative to the CO_2 injection. In the actual construction of numerical models, it is unrealistic to set infinite boundary conditions for numerical models from the viewpoint of computing time and modeling methods. Therefore, considering actual geological conditions, it is very important to determine a reasonable model scale for simulation accuracy and computational efficiency.

When CO_2 is injected into the reservoir, the pressure field will transmit mainly in the reservoir. According to the geological conditions in the study area, there is a fault zone near the existing shallow groundwater sources on the south of the target injection well. In order to explore the influence range of CO_2 injection on the reservoir pressure field in the horizontal direction and analyze the possible pressure increase in the deep reservoir in the distance of the area where the fault zone exists, a radial model with a radius of 100 km was set up. The purpose of using 100 km as the model radius is to ensure the fault zone is within the simulated area.

3.1. Exploration of the Boundary of Models. In this study, based on the geological conditions of the target reservoirs at the demonstration site, the extent and intensity of the influence of CO_2 injection on the reservoir pressure field are explored through a radial flow model. This exploration lays the foundation for the model scale and boundary setting in the construction of 3D models.

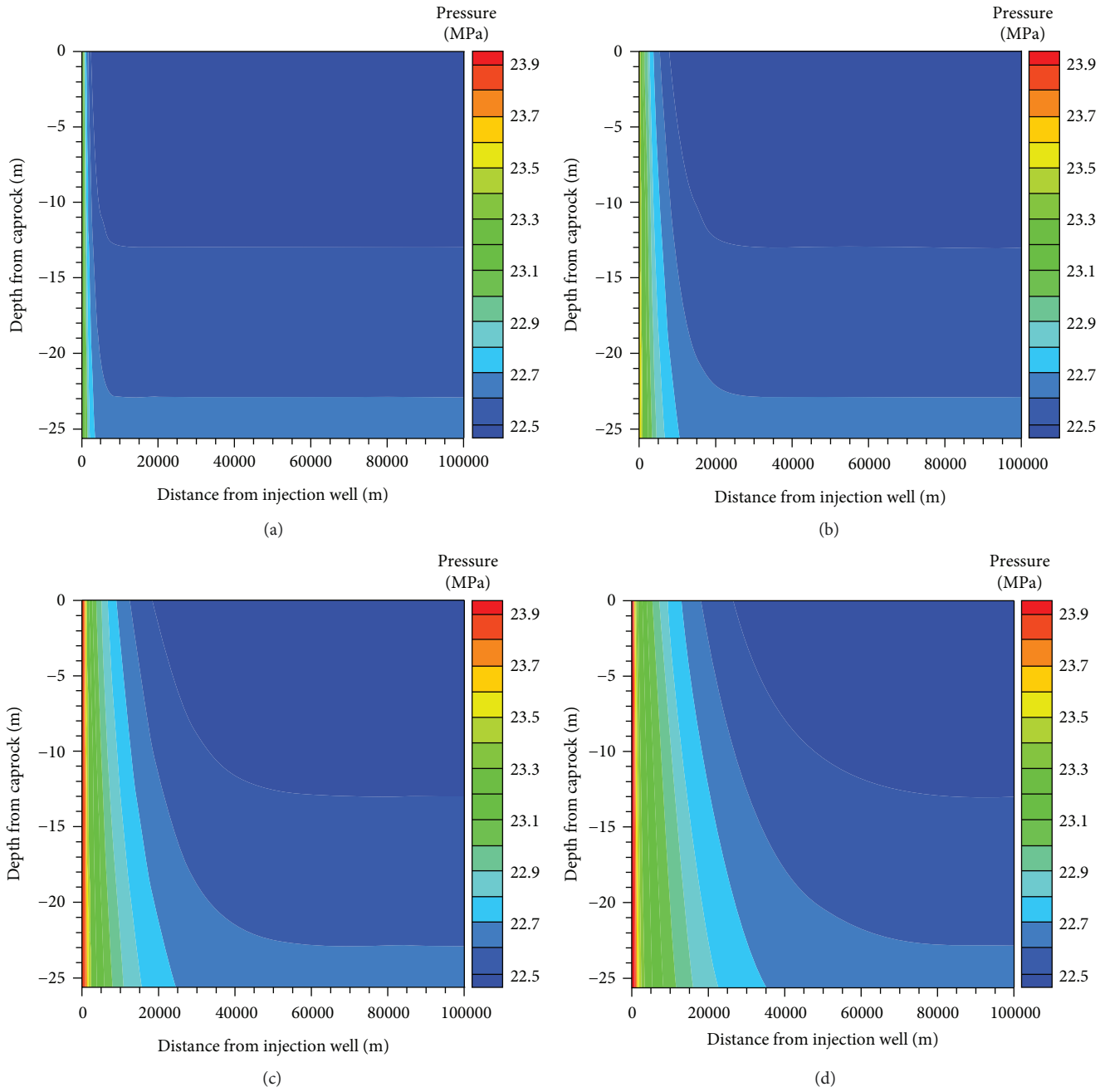

Figure 9: Evolution of the reservoir pressure field during injection in the radial model.

The simulations were carried out using the TOUGH2-MP/ECO2N code, the parallel version of TOUGH2 with the fluid property module ECO2N, which describes the non-isothermal flow of multiphase and multicomponent fluids in porous or faulted geologic media. ECO2N is a fluid property module for the TOUGH2 simulator (version 2.0) that was designed for applications for geologic sequestration of CO_2 in saline aquifers [26]. This module includes a comprehensive description of the thermodynamics and thermophysical properties of H_2O–NaCl–CO_2 mixtures and reproduces fluid properties largely within the experimental error for the temperature, pressure, and salinity conditions of interest ($10°C \le T \le 110°C$, $P \le 60$ MPa; and salinity up to full halite saturation).

3.1.1. Design of the Radial Model for Exploring Model Boundaries. To explore the range of the influence of CO_2 injection on the reservoir pressure field, a radial model of the deep saline aquifer is established according to the geological conditions of the target reservoir. The radial length of the model is 100 km, which is divided into 84 grids by means of unequal splitting. The vertical thickness of the reservoir is 25.625 m, which is divided into 18 layers according to porosity and permeability conditions. The radial model is shown in Figure 6.

Because of the very low porosity and low permeability of the formations at the top and bottom of this target reservoir, both the top boundary and bottom boundary of the model are set as impermeable barriers. To explore the influence of CO_2 injection on the reservoir pressure field in the process of CO_2 geological storage, the lateral boundary of the model is also set as a barrier.

The injection well penetrates the entire reservoir. Considering reservoir safety and injection efficiency, the pressure in the injection well is 1.3 times the original pressure in the reservoir. The injection time is set to 10 years according to the plan of the demonstration project. The total simulation time is 100 years based on previous research.

3.1.2. Model Parameters. According to the geological conditions of the site, the formation is generalized into horizontally isotropic sandstone formations. The reservoir was treated as a porous medium. Each grid block is specified with the following parameters: absolute permeability, porosity, rock density, thermal conductivity, and specific heat capacity, as well as the relative permeability and capillary pressure relationships [27]. The reservoir is a saline aquifer, and the concentration of total dissolved solids (TDS) in the groundwater is 43223.05 mg/L based on the analysis results of the actual reservoir groundwater. The initial temperature and the initial pressure of the reservoir are determined based on the actual measured value in the injection well. The rock density, thermal conductivity, and rock grain-specific heat are determined according to the rock test results from the target reservoir (Figure 7) and empirical parameters. The detailed parameters of the model are summarized in Table 1.

Relative permeability and capillary pressure are important physical parameters in the multiphase fluid seepage process. The definitions and values of the parameters are listed in Table 2.

The relative permeability of the liquid phase is calculated using the van Genuchten-Mualem relationship [28]:

$$k_{rl} = \sqrt{S^*}\left(1 - \left(1 - (S^*)^{1/m}\right)^m\right)^2, \quad (1)$$

$$S^* = \frac{S_l - S_{lr}}{S_{ls} - S_{lr}}. \quad (2)$$

To calculate the relative permeability for gas, the Corey function is used [29]:

$$k_{rg} = {}^2\left(1 - S\Lambda^2\right), \quad (3)$$

$$\widehat{S} = \frac{S_l - S_{lr}}{1 - S_{lr} - S_{gr}}. \quad (4)$$

The capillary pressure is calculated using the van Genuchten function:

$$P_{\text{cap}} = -P_0\left(\left[S^*\right]^{-1/m} - 1\right)^{1-m} \quad (5)$$

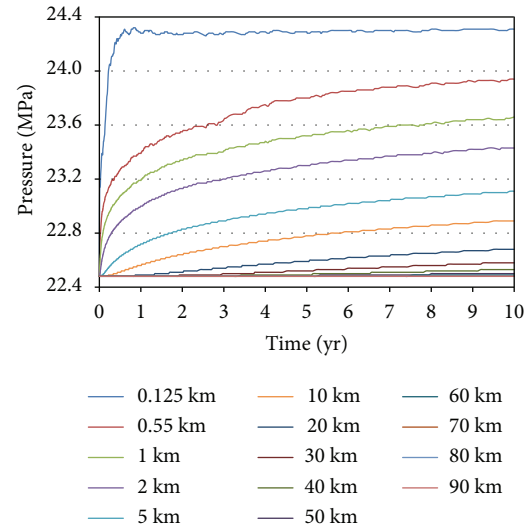

Figure 10: Pressure changes at pressure monitoring points during injection.

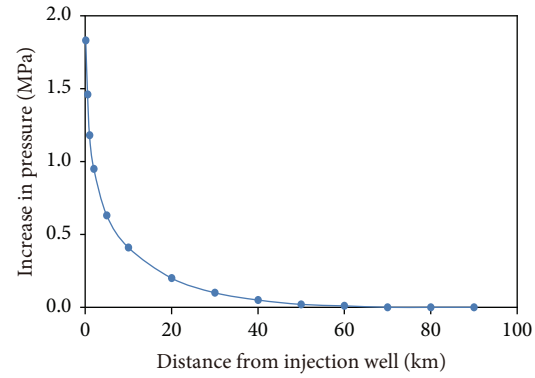

Figure 11: Pressure increases at the monitoring points during injection in the 10th year.

3.1.3. Pressure Monitoring Points in the Reservoir. To monitor the influence of CO_2 injection on the reservoir pressure field and provide a basis for setting the 3D model, the pressure monitoring points are placed at positions 0.125 km, 0.55 km, 1 km, 2 km, 5 km, 10 km, 20 km, 30 km, 40 km, 50 km, 60 km, 70 km, 80 km, and 90 km from the injection well, as shown in Figure 8. High-porosity and high-permeability formations are conducive to pressure field diffusion and CO_2 diffusion. To fully monitor the influence on the pressure field, the monitoring points are set at locations within the reservoir with high-porosity and high-permeability conditions, that is, at $Z = -18$ m below the reservoir caprock.

3.1.4. Evolution of the Pressure Field in the Reservoir. According to the evolution of the pressure field during the CO_2 injection process (Figure 9), the reservoir pressure continuously increases during CO_2 injection. The high-pressure zone is rapidly transferred from the injection well to surrounding areas within the reservoir. The range of influence continuously expands.

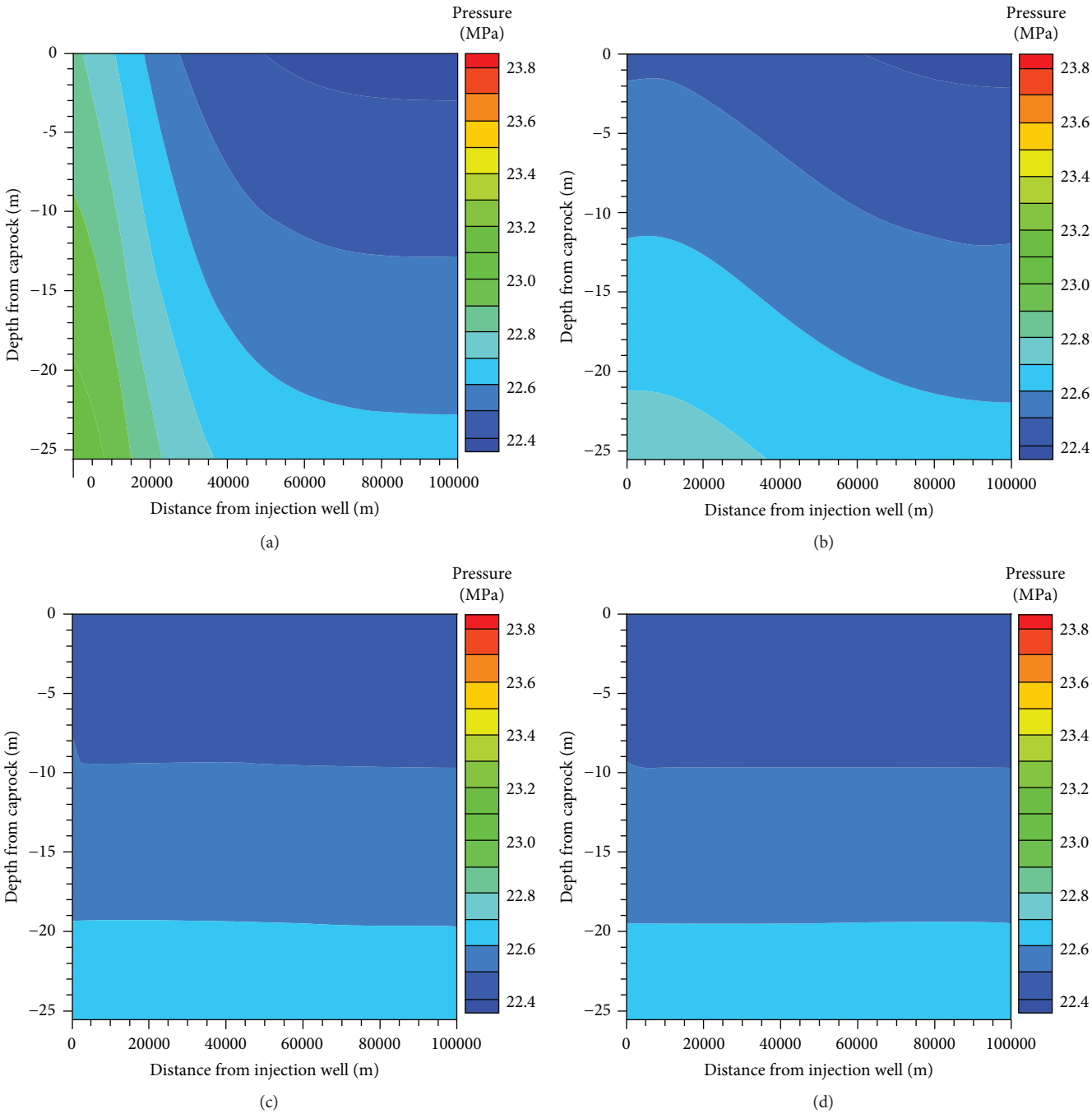

Figure 12: Evolution of the reservoir pressure field after the cessation of CO_2 injection.

The pressure changes at each pressure monitoring point (Figure 10) show that the closer the monitoring point is to the injection well, the more the pressure increases. At the same time, as the injection process progresses, the pressure at each monitoring point gradually stabilizes. The closer the monitoring point is to the injection well, the shorter the stabilization time is. At the pressure monitoring point 125 m from the injection well, after one year of injection, the pressure at this point no longer changes, stabilizing at approximately 24.30 MPa, and the reservoir pressure increase is 1.83 MPa. At the pressure monitoring point 1 km from the injection well, the reservoir pressure basically stabilizes after 9 years of injection and the reservoir pressure increase is 1.18 MPa. Compared to the pressure at the 125 m monitoring point, the pressure at the 1 km monitoring point takes longer to stabilize and the pressure increase is significantly less at the 1 km monitoring point than that at the 125 m monitoring point.

Comparing the pressure at the end of injection in the 10th year at different monitoring points with the initial pressure before the injection, the increases in pressure at different monitoring points can be obtained, as shown in Figure 11.

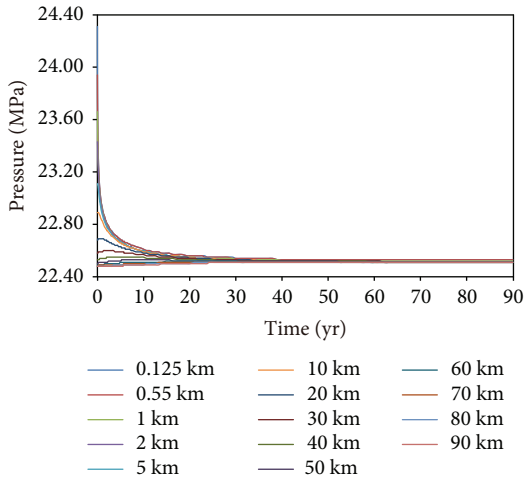

Figure 13: Pressure changes at pressure monitoring points after the cessation of CO_2 injection.

According to the pressure changes, as the distance between the monitoring point and the injection well increases, the pressure change rapidly decreases. Moreover, as the distance from the injection well increases, the pressure change rapidly decreases. At a distance of 0.125 km from the injection well, the pressure increase is as high as 1.83 MPa, while at a distance of 30 km from the injection well, the pressure increase is only 0.1 MPa. In formations more than 50 km from the injection well, there is virtually no change in formation pressure.

According to the change in the reservoir pressure field after the cessation of CO_2 injection (Figure 12), the accumulated pressure gradually dissipates after the CO_2 injection stops. After a certain period of time, the reservoir pressure gradually returns to the initial pressure.

After the CO_2 injection stops, the pressure at each pressure monitoring point changes, as shown in Figure 13. As seen in the figure, for 10 years after the cessation of CO_2 injection, the reservoir pressure decreases. After 30 years following the cessation of CO_2 injection, the formation pressure gradually returns to the initial formation pressure of approximately 22.50 MPa.

3.1.5. Diffusion and Distribution of CO_2 in the Reservoir. The CO_2 diffusion and distribution patterns during the injection process (Figure 14) reveal that after CO_2 is injected into the reservoir, lateral and vertical diffusion occurs under the combined action of gravity and buoyancy. When the injection stops, the maximum lateral diffusion distance of CO_2 is 1099 m.

The CO_2 distribution after the cessation of CO_2 injection is shown in Figure 15. CO_2 continues to undergo lateral and vertical diffusion under the combined effects of gravity and buoyancy. However, the pressure in the reservoir rapidly decreases. The pressure field in the reservoir gradually returns to its original state. The pressure difference at different positions driving CO_2 diffusion is also rapidly reduced. Therefore, the CO_2 diffusion rate declines significantly. After the injection stops, the CO_2 distribution does not change significantly. After 90 years following the cessation of the injection, the maximum CO_2 diffusion distance is 1329 m.

3.2. 3D Numerical Model of the Influence of CO_2 Injection on the Reservoir Pressure Field

3.2.1. Design of Models. Because the radial flow model simulation cannot simulate the evolution of the pressure field under the conditions of multiple injection wells, a 3D model for CO_2 injection into the Donggou Formation reservoir is constructed. The simulations were also carried out using the TOUGH2-MP/ECO2N code.

Although the influence distance of the injection reaches 50 km in the radial model, the pressure change is small. Even at a distance of 30 km from the injection well, the pressure change is only 0.1 MPa. Moreover, considering the distance between the injection well and the water source, the distance from the injection well to the model boundary is set to 30 km in the 3D model. The numerical model is set to 30 km in the X direction, 64 km in the Y direction, and 25.625 m in vertical thickness.

In the 1-well injection model (Figure 16), there are 27 layers in the X direction, 69 layers in the Y direction, and 18 layers in the vertical direction. In the injection model with two wells (Figure 17), there are 27 layers in the X direction, 70 layers in the Y direction, and 18 layers in the vertical direction. In the injection model with three wells (Figure 18), there are 27 layers in the X direction, 71 layers in the Y direction, and 18 layers in the vertical direction.

The top and bottom plates of the model are both water-resistant boundaries. The side boundaries on one side of the well are zero-flow boundaries. The three side boundaries without wells are constant-pressure boundaries. Combining the CO_2 diffusion distance and distribution in the CO_2 injection simulation of the target reservoir in the Donggou Formation, the injection well spacing is set to 2 km in the 2-well and 3-well models.

The porosity, permeability, temperature, and pressure of each reservoir in the model are the actual measured values from the target injection well and are the same as those used in the radial model. The values of the rock density, thermal conductivity, specific heat capacity, relative permeability, and capillary pressure in the model are also the same as those used in the radial model.

Each injection well penetrates the entire reservoir. The constant injection pressure mode is used, and the pressure in the injection well is 1.3 times the original pressure in the reservoir. The injection time is 10 years, and the total simulation time is 100 years.

3.2.2. Pressure Monitoring Points in the Reservoir. To monitor the influence of CO_2 injection on the reservoir pressure field, the pressure monitoring points are set at positions 0.6 km, 1.25 km, 3 km, 5.5 km, 11 km, 20 km, and 25 km from the injection well, as shown in Figure 19 in the 1-well model. High-porosity and high-permeability formations are conducive to pressure field diffusion and CO_2 diffusion. To fully monitor the influence on the pressure field, the monitoring points are set at locations within the reservoir with the

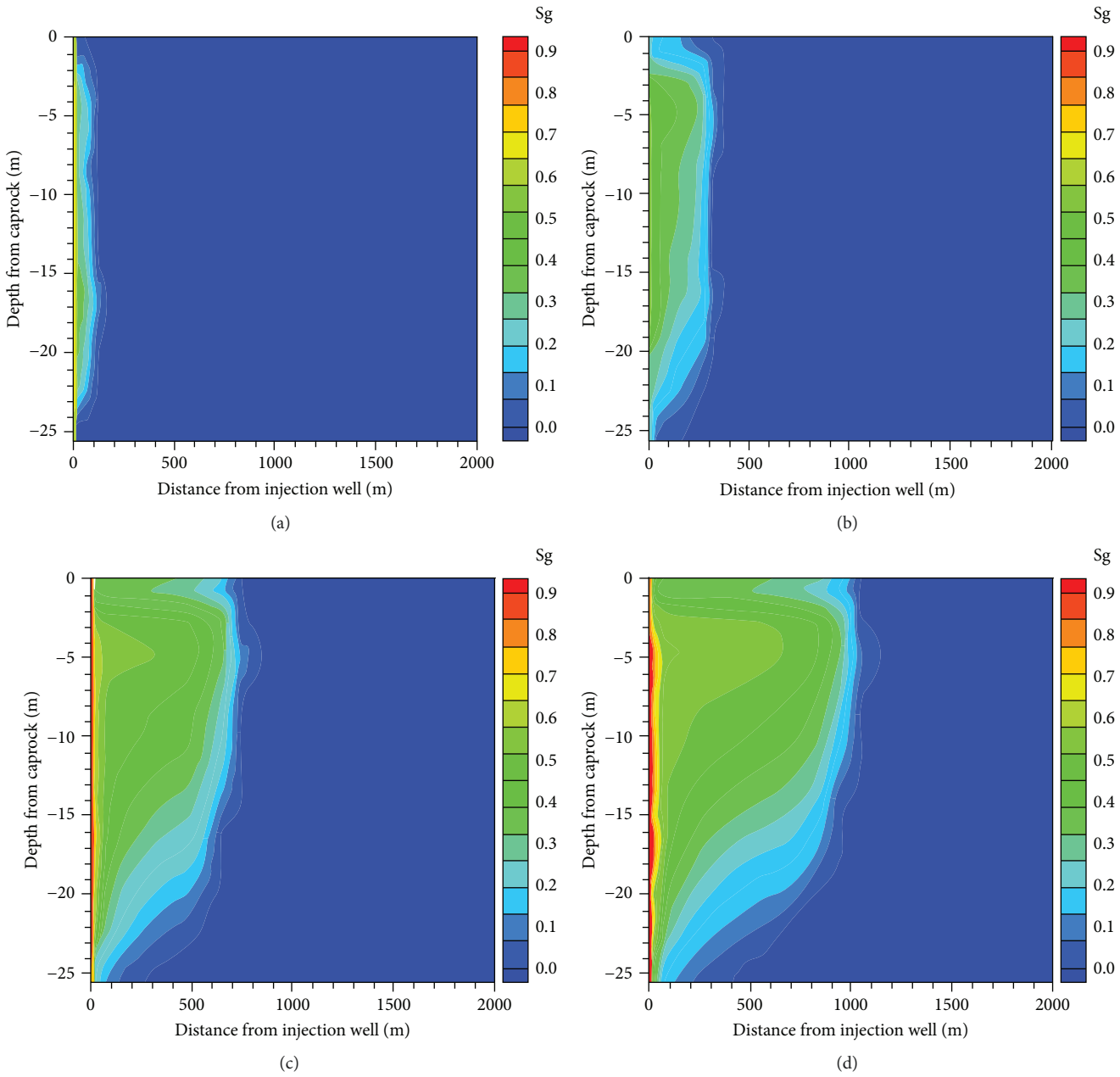

Figure 14: Spatial distributions of supercritical CO_2 during injection (Sg: gas saturation of CO_2).

highest porosity and permeability conditions, that is, at $Z = -18$ m below the reservoir caprock.

In the 1-well model, the pressure monitoring points are shown in Figure 19. In the 2-well model, the pressure monitoring points are divided into two rows, which extend away from vertical well 1 and from a point between the two wells. The monitoring points constitute two pressure monitoring lines, which are shown in Figure 20. In the 3-well model, the pressure monitoring points are also divided into two rows, which extend away from vertical wells 1 and 2 and form two pressure monitoring lines. The locations are shown in Figure 21.

3.2.3. Evolution of the Pressure Field during CO_2 Injection. The pressure changes in the reservoir are caused by the CO_2 injection. The injection rate of every model and the total injection amount for each injection model are shown in Figures 22 and 23. The total CO_2 injection rates were stable at 5.8, 9.6, and 12.4 kg/s to the single well, double wells, and three wells, respectively. During the 10-year injection period, the total injection amounts were 1.81, 3.05, and 3.98 million tons, respectively.

According to the simulation results, the pressure changes at the pressure monitoring points in the models with 1, 2, and 3 wells are shown in Figures 24–26. As with the radial model, there is a positive correlation between the pressure increment and the distance from the monitoring points to the injection well. At the same time, as the injection process progresses, the pressure at each monitoring point gradually stabilizes. At monitoring points

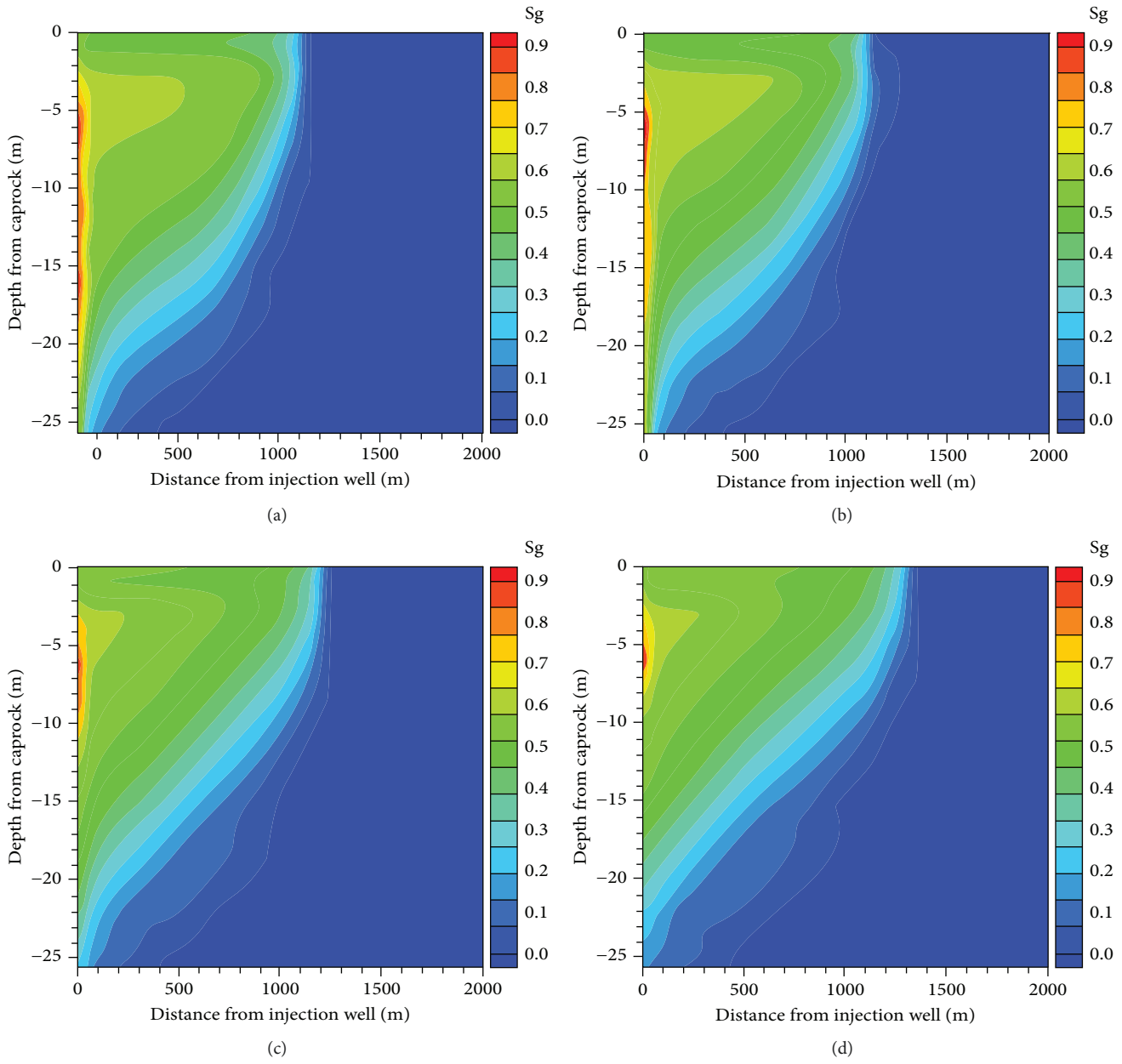

Figure 15: Spatial distributions of supercritical CO_2 after injection cessation (Sg: gas saturation of CO_2).

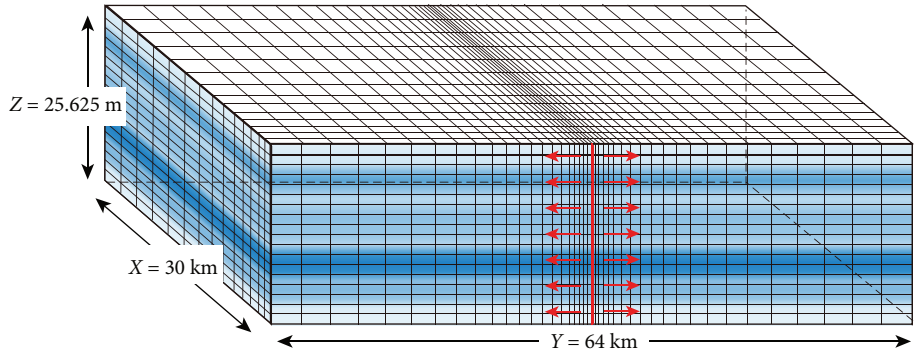

Figure 16: 3D model of one injection well.

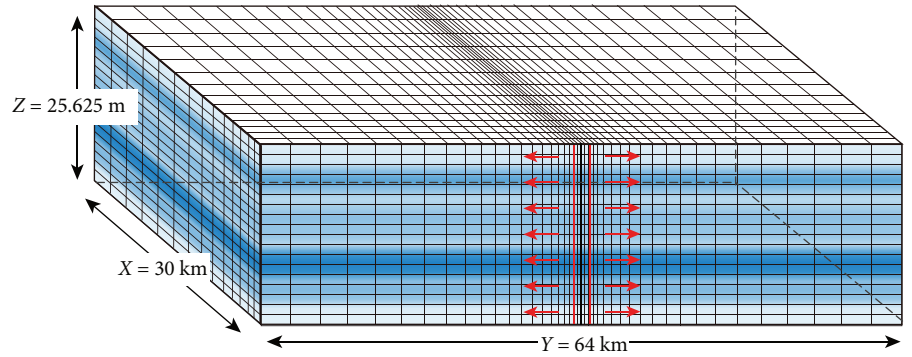

Figure 17: 3D model of 2 injection wells.

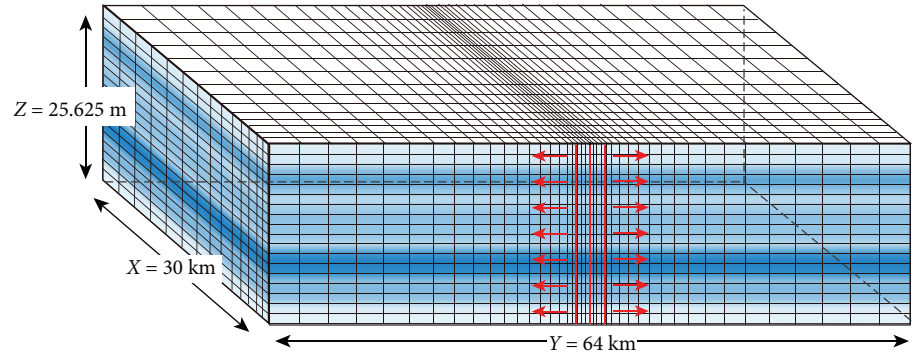

Figure 18: 3D model of 3 injection wells.

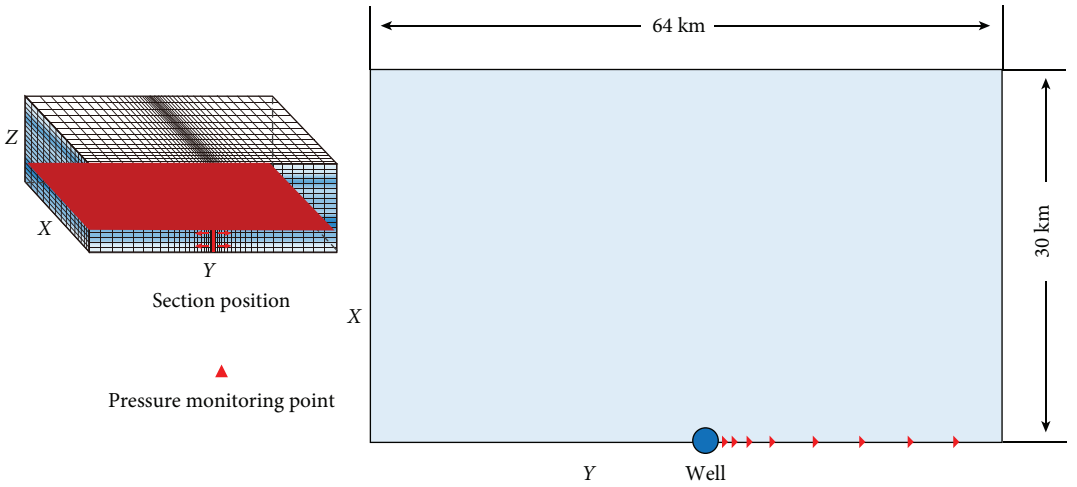

Figure 19: Locations of the pressure monitoring points in the 1-well model.

that are closer to the injection well, the pressure basically stabilizes over a shorter time.

To analyze the influence of CO_2 injection on the reservoir pressure field under the conditions of different numbers of injection wells, the effects of the number of injection wells on the pressure change are compared. In the 2-well and 3-well models, the degree of pressure change along the pressure monitoring line exhibits relatively large changes. The pressure changes at different distances from the injection well(s) for different numbers of injection wells are shown in Figure 27. The void space is constant for a fixed-volume reservoir. During the injection process, more injection wells can fill the pore space near the injection well at a faster rate and cause the pressure to increase faster than the circumstance with the lesser number of injection wells. And this makes the fluid move outward faster in the reservoir. Thus, more injection wells in operation simultaneously can produce more pressure buildup at the same time and the same location in the reservoir than a single-well injection.

Taking the change in the pressure field for the 1-well model as an example, the distribution of pressure changes at the pressure monitoring points demonstrates that the

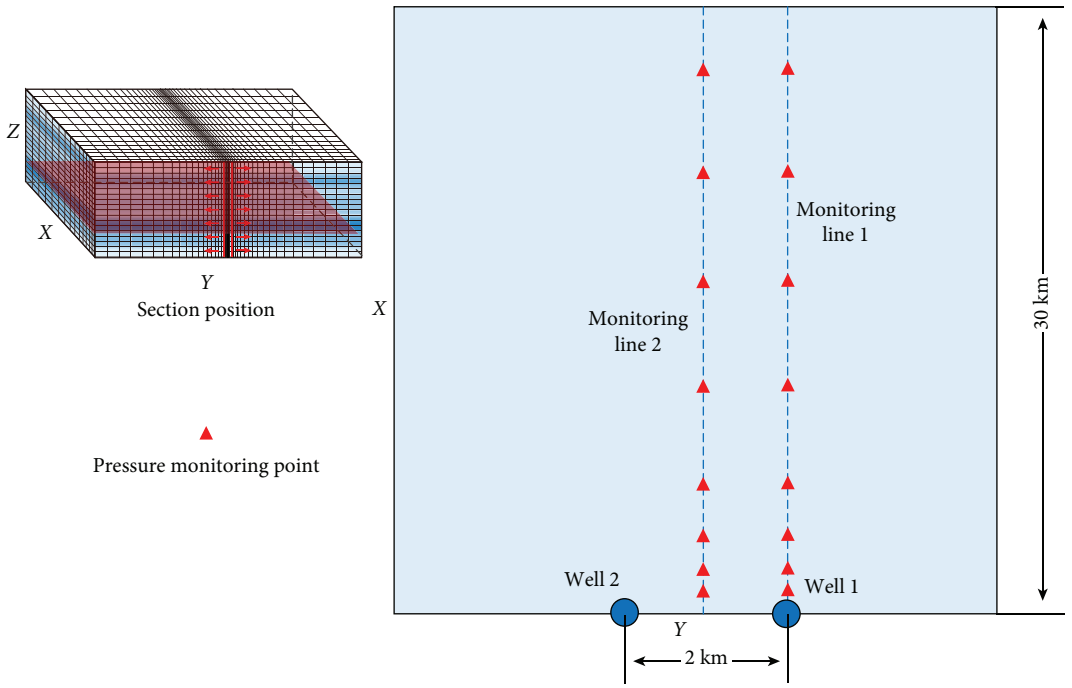

Figure 20: Positions of the pressure monitoring points in the 2-well model.

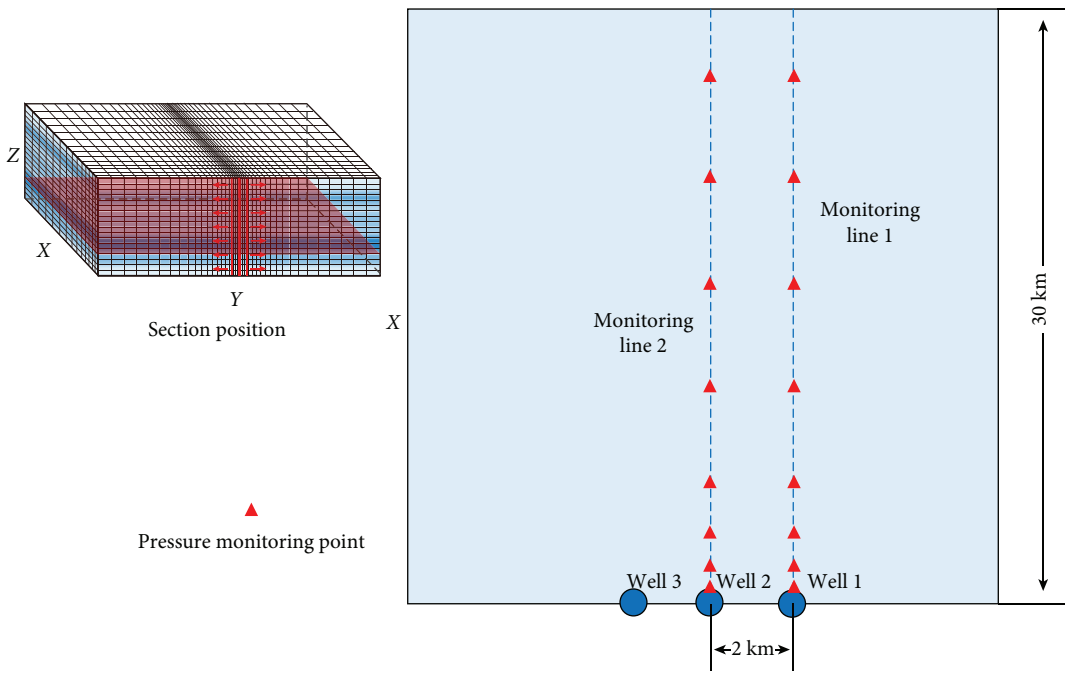

Figure 21: Positions of the pressure monitoring points in the 3-well model.

closer the monitoring point is to the injection well, the greater the pressure increase is. As the distance between the pressure monitoring point and the injection well increases, the pressure change rapidly decreases. At a distance of 0.6 km from the injection well, the pressure increase is as high as 1.1 MPa. However, at 25 km from the injection well, the pressure increase is only 0.03 MPa.

A comparison of the reservoir pressure changes for models with different numbers of injection wells shows that the number of injection wells has a significant effect on reservoir pressure changes. At a distance of 0.6 km from the injection well, the pressure increase in the 1-well model is 1.10 MPa. The pressure increments of the monitoring points at the same distance in the 2-well model and the 3-well model are 1.58 MPa and 2.11 MPa, which are 1.43 and 1.92 times the pressure increment in the 1-well model, respectively. At monitoring points at different distances from the injection well, the magnitude of the pressure change under Mitsui

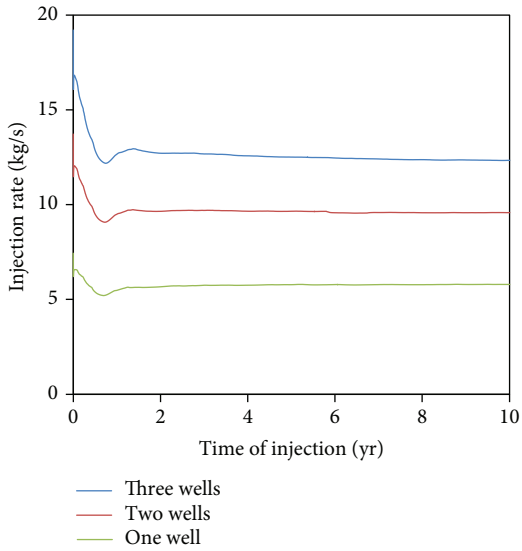

Figure 22: Injection rate of every model.

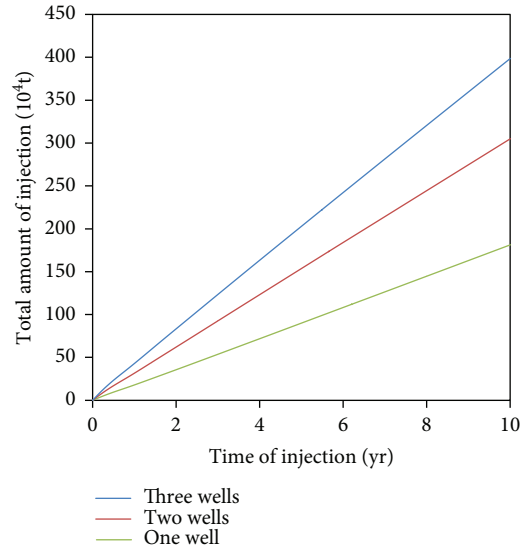

Figure 23: Total amount of CO_2 injected.

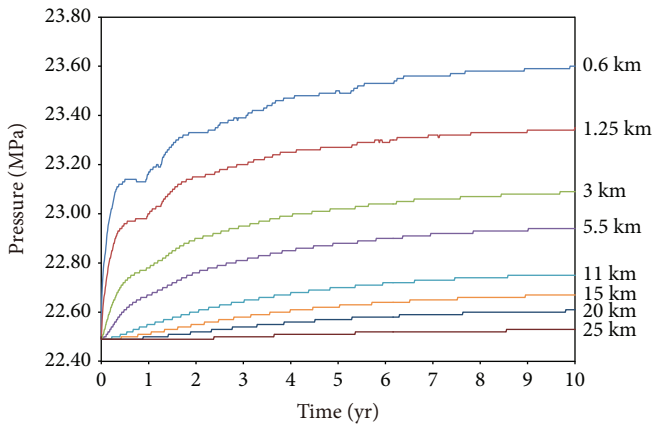

Figure 24: Pressure changes at the pressure monitoring points during injection in the 1-well model.

conditions can be two to three times more than that of the 1-well model. The more the injection wells, the more significant the impact on the reservoir pressure field is and the greater the pressure change is.

In the study of Zhao et al. [25], the authors injected CO_2 at a fixed rate method. Therefore, the reservoir pressure changes in this study are smaller than those of Zhao et al. The maximum pressure buildup in the formation ranges from 8.6 MPa to 9.3 MPa. However, the influence of CO_2 injection on the pressure field is not much different. Due to the longer simulation time studied by Zhao et al., the CO_2 diffusion distance in the reservoir is significantly larger than that in this study. The maximum-extent distance of the CO_2 plume from different injection wells is more than 4 km, which is mainly determined by the permeability and structure of the formation.

3.2.4. Evolution of the Pressure Field after Stopping CO_2 Injection. In the 1-well injection model, the changes in pressure at each pressure monitoring point after CO_2 injection cessation are shown in Figure 28. The pressure accumulated in the reservoir gradually dissipates after CO_2 injection cessation. After a certain period of time, the reservoir pressure field slowly returns to the initial pressure field state.

According to the pressure changes under the conditions of the 1-well model (Figure 28), 2-well model (Figure 29), and 3-well model (Figure 30), the reservoir pressure decreases rapidly after CO_2 injection ceases. By 10-15 years after the cessation of the injection process, the reservoir pressures in the different injection well models are restored to the initial reservoir pressure.

When the pressure change of the reservoir is less than 0.05 MPa (2‰ of the initial reservoir pressure), it is considered to return to the initial pressure state. Under such conditions, the time required for the pressure at monitoring points at different distances from the injection well to return to the initial pressure is shown in Table 3.

During the period after the injection ceases, regardless of the number of wells, the nearer area to the injection well, the longer time the needed to recover to the initial reservoir pressure and the shorter the recovery time needed for the far area. For example, to the single-well mode, the pressure recovery time at 0.6 km is 8.1 years and the pressure recovery time at 20 km is 5.4 years. This is mainly because there is more pressure accumulation in the near area to the injection well, and the pressure dissipation process is longer than that in the far area where the pressure accumulation is small.

At the same distance from the injection well, the time of pressure recovery is positively correlated with the number of injection wells. However, the difference in recovery time is not particularly obvious. For example, at a distance of 1.25 km from the injection well, reservoir pressure recovery time is 8.1 years (one injection well), 9.2 years (two injection wells), and 10.4 years (three injection wells), with a maximum difference of 2.3 years (Table 3).

After the 10 years of injection was ceased, the reservoir pressure basically returned to its initial pressure state. The CO_2 loses its drive force in the reservoir, and the storage mechanism gradually shifts to other mechanisms such as dissolved storage and mineral storage.

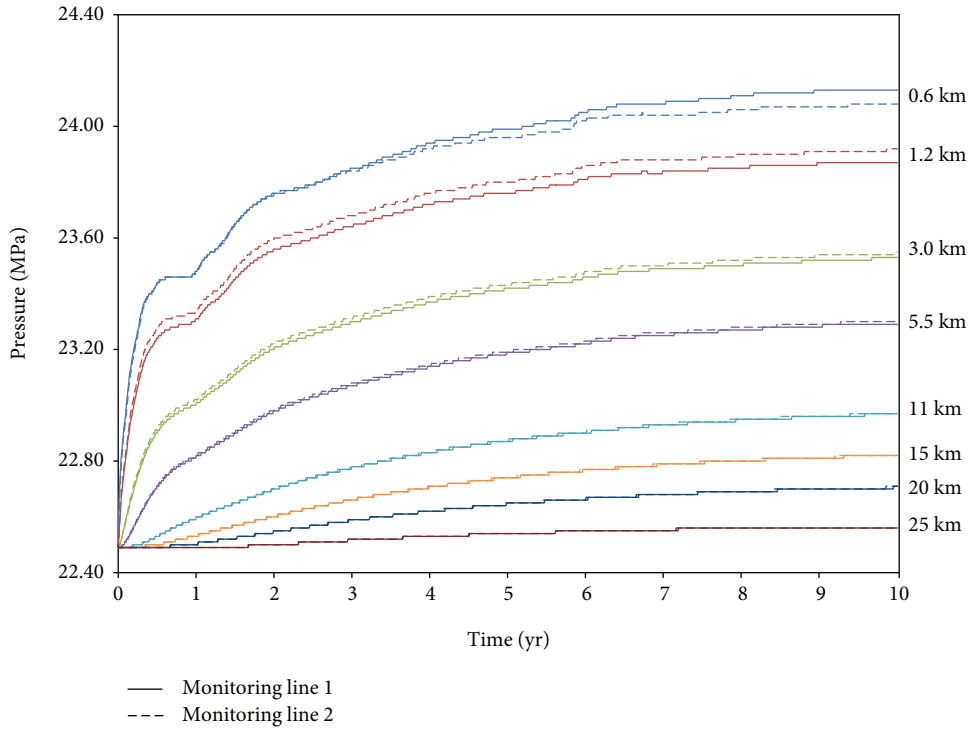

Figure 25: Pressure changes at the pressure monitoring points during injection in the 2-well model.

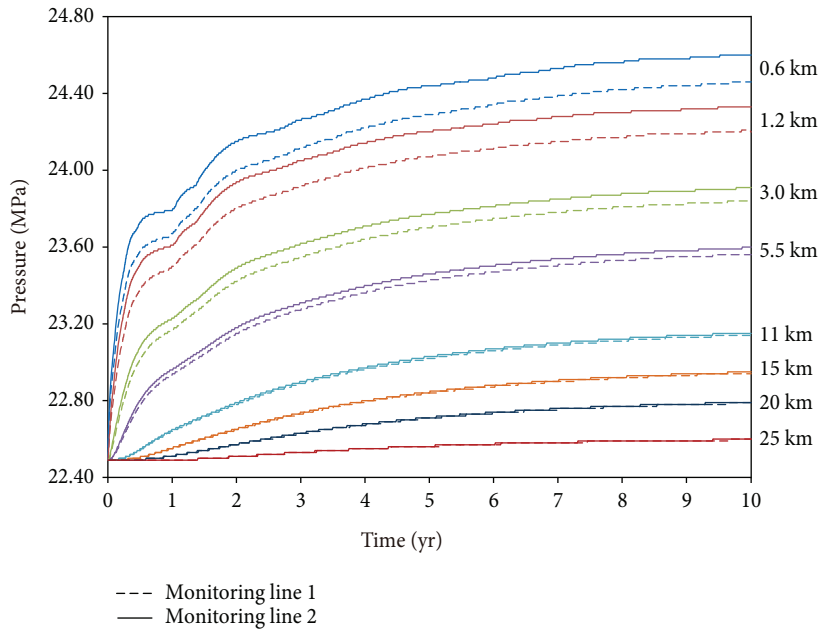

Figure 26: Pressure changes at the pressure monitoring points during injection in the 3-well model.

3.3. The Impact of CO_2 Injection on the Safety of Groundwater. In the radial model, after CO_2 is injected into the reservoir, gravity and buoyancy forces cause lateral and vertical CO_2 diffusion. However, under the injection pressure equivalent to 1.3 times the reservoir pressure, the maximum lateral diffusion distance of CO_2 is 1329 m after a simulation time of 100 years. Due to the small CO_2 diffusion distance, CO_2 cannot migrate to the groundwater source area near the study area, which is 25-40 km from the injection well. Therefore, CO_2 diffusion in the target reservoir will not affect the water quality of the water source.

The large-scale injection of CO_2, especially via multiple injection wells, has a larger effect on the pressure field in the reservoir than on the CO_2 diffusion distance. However, the effect of CO_2 injection on the pressure field is most evident in the regions close to the injection well. As the distance from

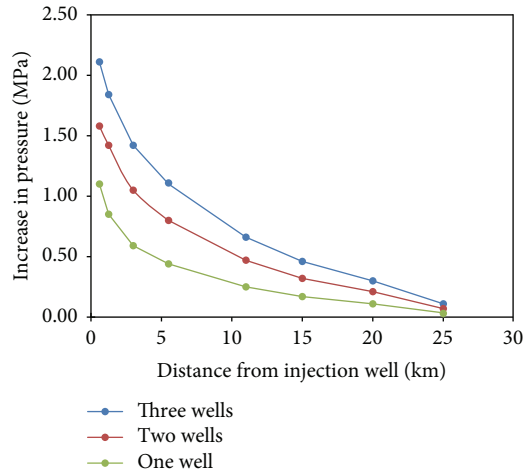

Figure 27: Pressure changes at the pressure monitoring points in models with different numbers of wells in the 10th year.

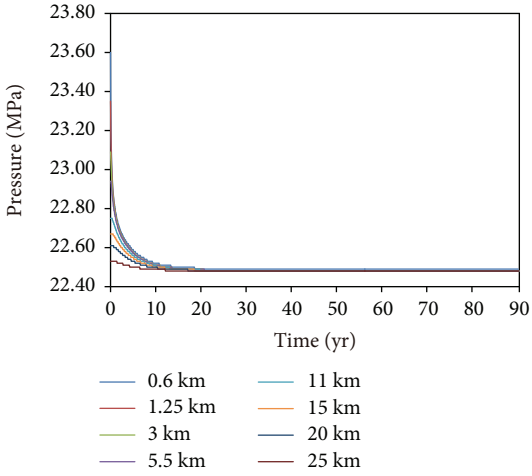

Figure 28: Pressure changes at the pressure monitoring points after cessation of CO_2 injection in the 1-well model.

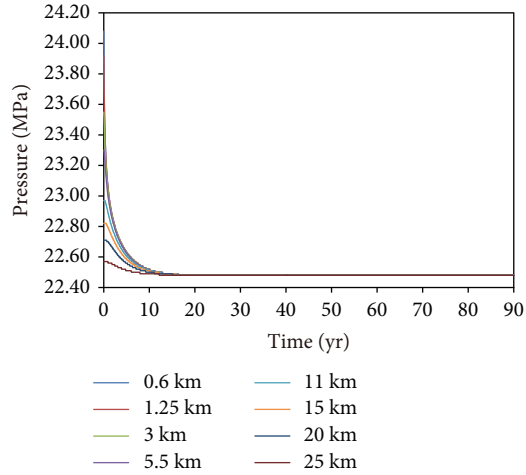

Figure 29: Pressure changes at the pressure monitoring points after cessation of CO_2 injection in the 2-well model.

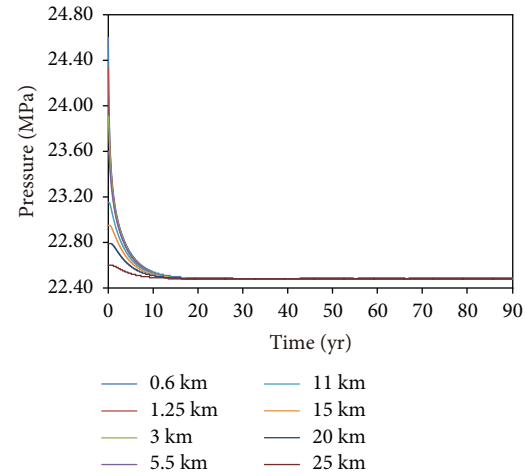

Figure 30: Pressure changes at the pressure monitoring points after cessation of CO_2 injection in the 3-well model.

Table 3: The time it takes for the pressure at monitoring points at different distances from the injection well to return to the initial pressure (time: yr).

Distance from injection well (km)	0.6	1.25	3	5.5	11	15	20	25
One-injection well model	8.1	8.1	8.1	8.1	7.5	6.6	5.4	1.3
Two-injection well model	9.2	9.2	9.3	9.2	8.7	8.0	7.0	3.9
Three-injection well model	10.4	10.4	10.5	10.4	10.0	9.3	8.3	5.1

the injection well increases, the pressure change in the reservoir decreases rapidly. In the 1-well injection conditions of the radial model, the pressure increase in the reservoir is only 0.1 MPa at 30 km from the injection well. In the 3D model with different numbers of injection wells, under 1-well, 2-well, and 3-well conditions, the pressure increases at a distance of 25 km from the injection well are only 0.03 MPa, 0.07 MPa, and 0.11 MPa, respectively. Under the 3-well conditions, when the injection time is 10 years, the injection has the greatest influence on the reservoir pressure field. The influence distance on the pressure field and the pressure increase in the reservoir at this time are shown in Figure 31.

The groundwater sources in the study area are 25-40 km from the target injection well, and CO_2 injection has a very low impact on the pressure field in the reservoir of the water source area. In addition, the exploitation of groundwater sources occurs mainly in the Quaternary unconfined aquifer and shallow confined aquifer and there are multiple sets of reservoir-caprock combinations between the CO_2 injection level and the exploited water resources. The mining horizon of the water source is approximately 1600 m apart from the CO_2 reservoir. Therefore, it would be difficult for the pressure propagation after CO_2 injection to affect the groundwater dynamic field in the shallow confined aquifers and aquifers. The threat to the water supply safety and water quality safety of water sources can be ignored.

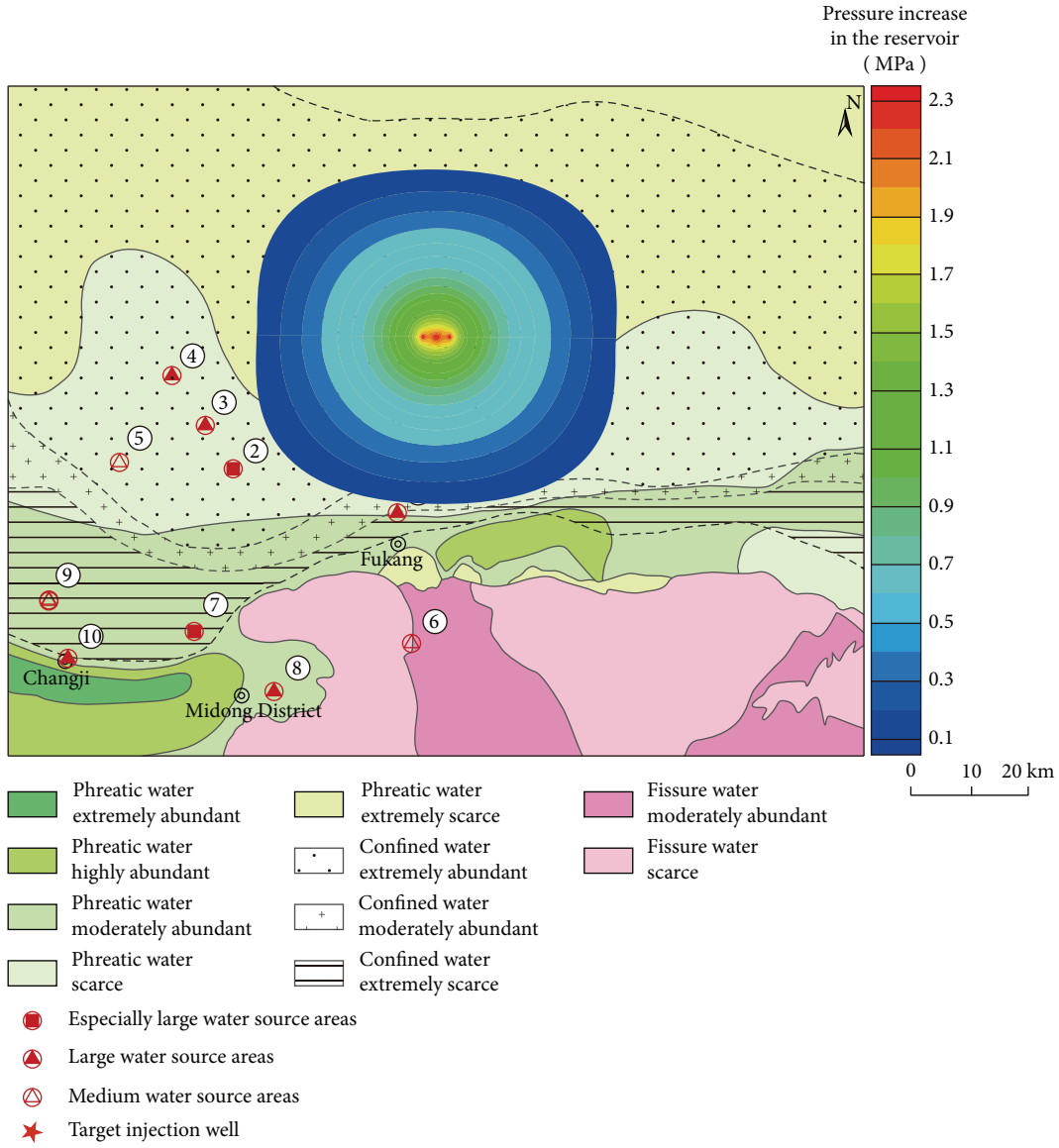

FIGURE 31: Pressure increase in the CO_2 reservoir when injection ceases in the 10th year in the 3-well model.

4. Conclusions and Suggestions

This paper studied the demonstration site for CO_2-enhanced water recovery technology in the Junggar Basin and selected the Cretaceous Donggou Formation as the target reservoir. The CO_2 diffusion and reservoir pressure field changes caused by CO_2 injection via different numbers of injection wells were analyzed by numerical simulation. The following conclusions were obtained:

(1) The influence distance of CO_2 injection on the target reservoir pressure field in the 1-well model was explored through a radial model. Under an injection pressure of 1.3 times the reservoir pressure, the pressure change at a distance of 30 km from the injection well was 0.1 MPa within the 10-year injection period and the reservoir pressure at 50 km was not changed. This result provided a scientific basis for the 3D model scaling and the setting of boundary conditions

(2) The 3D model was used to explore the pressure field evolution of the reservoir. The results showed that during the injection period, the pressure field continuously expanded. The closer the distance to the injection well, the higher the variability of pressure was. As the distance increased, the pressure change decreased rapidly. After the injection ceased, the reservoir pressure completely recovered to the initial reservoir pressure after 15 years

(3) At the same injection pressure, the number of injection wells had a significant effect on the evolution of reservoir pressure. As the number of injection wells increased, the pressure increase at the monitoring points at the same distance from the injection well increased significantly. At monitoring points at

different distances from the injection well, the amount of pressure change under Mitsui conditions was two to three times more than that of a 1-well situation. When the injection of CO_2 ceased, the reservoir pressure returned to its initial pressure level after 10-15 years. The recovery time was not significantly related to the number of injection wells

(4) According to the results of the numerical simulation, due to the small CO_2 diffusion distance, the large-scale injection of CO_2 will not affect the groundwater quality in the water source area. The extent of the pressure field change caused by CO_2 injection is much greater than the extent of CO_2 diffusion. However, the reservoir pressure field near the water source changes very little. The impact of CO_2 injection on the shallow groundwater dynamics on the southern side of the Tian Shan Mountains can therefore be ignored. The scaled injection of CO_2 in the study area will not have a significant impact on the development and utilization of groundwater from nearby water sources

The current simulation results are only based on the 10-year fixed pressure injection. If the project's operating period is extended, the impact of CO_2 injection on the hydrodynamic field will increase. Under the joint of geological structures such as faults, the characteristics of groundwater hydrochemistry and the hydrodynamic field in the shallow surrounding area might be changed, which may affect the safety of the water supply.

Data Availability

The data used to support the findings of this study are available from the corresponding author upon request.

Conflicts of Interest

The authors declare that there is no conflict of interest regarding the publication of this paper.

Acknowledgments

This work was supported by a China National Science and Technology Major Project (grant no. 2016ZX05016-005), a Geological Survey Project (grant no. 121201012000150010), and a Graduate Innovation Fund of Jilin University (grant no. 101832018C056). The paper was also supported by the Key Laboratory of Groundwater Resources and Environment (Jilin University), Ministry of Education, China, and by the Jilin Provincial Key Laboratory of Water Resources and Environment, Jilin University.

References

[1] D. Y. C. Leung, G. Caramanna, and M. M. Maroto-Valer, "An overview of current status of carbon dioxide capture and storage technologies," *Renewable and Sustainable Energy Reviews*, vol. 39, pp. 426–443, 2014.

[2] S. Bachu, "CO_2 storage in geological media: role, means, status and barriers to deployment," *Progress in Energy and Combustion Science*, vol. 34, no. 2, pp. 254–273, 2008.

[3] H.-H. Qiu and L.-G. Liu, "A study on the evolution of carbon capture and storage technology based on knowledge mapping," *Energies*, vol. 11, no. 5, p. 1103, 2018.

[4] E. A. Al-Khdheeawi, S. Vialle, A. Barifcani, M. Sarmadivaleh, and S. Iglauer, "Enhancement of CO_2 trapping efficiency in heterogeneous reservoirs by water-alternating gas injection," *Greenhouse Gases: Science and Technology*, vol. 8, no. 5, pp. 920–931, 2018.

[5] M. Z. Hasanvand, M. A. Ahmadi, S. R. Shadizadeh, R. Behbahani, and F. Feyzi, "Geological storage of carbon dioxide by injection of carbonated water in an Iranian oil reservoir: a case study," *Journal of Petroleum Science and Engineering*, vol. 111, pp. 170–177, 2013.

[6] F. Wang, J. Jing, T. Xu, Y. Yang, and G. Jin, "Impacts of stratum dip angle on CO_2 geological storage amount and security," *Greenhouse Gases: Science and Technology*, vol. 6, no. 5, pp. 682–694, 2016.

[7] S. Krevor, C. Reynolds, A. Al-Menhali, and B. Niu, "The impact of reservoir conditions and rock heterogeneity on CO_2-brine multiphase flow in permeable sandstone," *Petrophysics*, vol. 57, pp. 12–18, 2016.

[8] R. Juanes, E. J. Spiteri, F. M. Orr Jr, and M. J. Blunt, "Impact of relative permeability hysteresis on geological CO_2 storage," *Water Resources Research*, vol. 42, no. 12, 2006.

[9] N. Zhao, T. Xu, K. Wang, H. Tian, and F. Wang, "Experimental study of physical-chemical properties modification of coal after CO2 sequestration in deep unmineable coal seams," *Greenhouse Gases: Science and Technology*, vol. 8, no. 3, pp. 510–528, 2018.

[10] Q. Zhou, J. T. Birkholzer, C.-F. Tsang, and J. Rutqvist, "A method for quick assessment of CO_2 storage capacity in closed and semi-closed saline formations," *International Journal of Greenhouse Gas Control*, vol. 2, no. 4, pp. 626–639, 2008.

[11] E. A. Al-Khdheeawi, S. Vialle, A. Barifcani, M. Sarmadivaleh, and S. Iglauer, "The effect of $WACO_2$ ratio on CO_2 geo-sequestration efficiency in homogeneous reservoirs," *Energy Procedia*, vol. 154, pp. 100–105, 2018.

[12] E. A. Al-Khdheeawi, S. Vialle, A. Barifcani, M. Sarmadivaleh, Y. Zhang, and S. Iglauer, "Impact of salinity on CO_2 containment security in highly heterogeneous reservoirs," *Greenhouse Gases: Science and Technology*, vol. 8, no. 1, pp. 93–105, 2018.

[13] D. Liu, R. Agarwal, and Y. Li, "Numerical simulation and optimization of CO_2-enhanced water recovery by employing a genetic algorithm," *Journal of Cleaner Production*, vol. 133, pp. 994–1007, 2016.

[14] T. Kabera and Y. L. Li, "Injecting CO_2 and pumping out saline formation water simultaneously to control pressure build-up while storing CO_2 in deep saline aquifers," *Defect and Diffusion Forum*, vol. 332, pp. 63–75, 2012.

[15] M. A. Ahmadi, B. Pouladi, and T. Barghi, "Numerical modeling of CO_2 injection scenarios in petroleum reservoirs: application to CO_2 sequestration and EOR," *Journal of Natural Gas Science and Engineering*, vol. 30, pp. 38–49, 2016.

[16] J.-P. Nicot, "Evaluation of large-scale CO_2 storage on freshwater sections of aquifers: an example from the Texas Gulf Coast Basin," *International Journal of Greenhouse Gas Control*, vol. 2, no. 4, pp. 582–593, 2008.

[17] J. T. Birkholzer and Q. Zhou, "Basin-scale hydrogeologic impacts of CO_2 storage: capacity and regulatory implications," *International Journal of Greenhouse Gas Control*, vol. 3, no. 6, pp. 745–756, 2009.

[18] R.-R. ZHAO, Q.-H. MENG, and J.-M. CHENG, "Fluid migration modeling of CO_2 injection in deep saline aquifers-a case study of the Sanzhao Depression, Songliao Basin," *Rock and Soil Mechanics*, vol. 4, p. 44, 2012.

[19] H. Yamamoto, K. Zhang, K. Karasaki, A. Marui, H. Uehara, and N. Nishikawa, "Numerical investigation concerning the impact of CO_2 geologic storage on regional groundwater flow," *International Journal of Greenhouse Gas Control*, vol. 3, no. 5, pp. 586–599, 2009.

[20] J. T. Birkholzer, C. M. Oldenburg, and Q. Zhou, "CO_2 migration and pressure evolution in deep saline aquifers," *International Journal of Greenhouse Gas Control*, vol. 40, pp. 203–220, 2015.

[21] Y. Duan, N. Li, H. Mu, and S. Gui, "Research on CO_2 emission reduction mechanism of China's iron and steel industry under various emission reduction policies," *Energies*, vol. 10, no. 12, p. 2026, 2017.

[22] D. Li, D. He, M. Santosh, D. Ma, and J. Tang, "Tectonic framework of the northern Junggar Basin part I: the eastern Luliang Uplift and its link with the East Junggar terrane," *Gondwana Research*, vol. 27, no. 3, pp. 1089–1109, 2015.

[23] H. Yang, L. Chen, and Y. Kong, "A novel classification of structural units in Junggar Basin," *Xinjiang Petroleum Geology*, vol. 25, pp. 686–688, 2004.

[24] B.-Q. Zhu, Y. Gao, and X.-J. Meng, "Natural water quality and its suitability in the northern Tianshan catchments (Central Asia)," *Hydrology*, vol. 6, no. 1, pp. 32–42, 2018.

[25] R. Zhao, J. Cheng, K. Zhang, N. Liu, and F. Xu, "Numerical investigation of basin-scale storage of CO_2 in saline aquifers of Songliao Basin, China," *Greenhouse Gases: Science and Technology*, vol. 5, no. 2, pp. 180–197, 2015.

[26] K. Pruess and N. Spycher, "ECO2N–a fluid property module for the TOUGH2 code for studies of CO_2 storage in saline aquifers," *Energy Conversion and Management*, vol. 48, no. 6, pp. 1761–1767, 2007.

[27] Z. Yang, T. Xu, F. Wang, Y. Yang, X. Li, and N. Zhao, "Impact of inner reservoir faults on migration and storage of injected CO_2," *International Journal of Greenhouse Gas Control*, vol. 72, pp. 14–25, 2018.

[28] M. T. Van Genuchten, "A closed-form equation for predicting the hydraulic conductivity of unsaturated soils 1," *Soil Science Society of America Journal*, vol. 44, no. 5, pp. 892–898, 1980.

[29] A. T. Corey, "The interrelation between gas and oil relative permeabilities," *Producers Monthly*, vol. 19, pp. 38–41, 1954.